The Exceptionally Warm Winter of 2015/16 in Alaska

JOHN E. WALSH,[a] PETER A. BIENIEK,[b] BRIAN BRETTSCHNEIDER,[a] EUGÉNIE S. EUSKIRCHEN,[c] RICK LADER,[a,b] AND RICHARD L. THOMAN[d]

[a] *Alaska Center for Climate Assessment and Policy, University of Alaska, Fairbanks, Alaska*
[b] *Alaska Climate Science Center, University of Alaska, Fairbanks, Alaska*
[c] *Institute of Arctic Biology, University of Alaska, Fairbanks, Alaska*
[d] *NOAA/National Weather Service, Fairbanks, Alaska*

(Manuscript received 27 June 2016, in final form 28 November 2016)

ABSTRACT

Alaska experienced record-setting warmth during the 2015/16 cold season (October–April). Statewide average temperatures exceeded the period-of-record mean by more than 4°C over the 7-month cold season and by more than 6°C over the 4-month late-winter period, January–April. The record warmth raises two questions: 1) Why was Alaska so warm during the 2015/16 cold season? 2) At what point in the future might this warmth become typical if greenhouse warming continues? On the basis of circulation analogs computed from sea level pressure and 850-hPa geopotential height fields, the atmospheric circulation explains less than half of the anomalous warmth. The warming signal forced by greenhouse gases in climate models accounts for about 1°C of the anomalous warmth. A factor that is consistent with the seasonal and spatial patterns of the warmth is the anomalous surface state. The surface anomalies include 1) above-normal ocean surface temperatures and below-normal sea ice coverage in the surrounding seas from which air advects into Alaska and 2) the deficient snowpack over Alaska itself. The location of the maximum of anomalous warmth over Alaska and the late-winter–early-spring increase of the anomalous warmth unexplained by the atmospheric circulation implicates snow cover and its albedo effect, which is supported by observational measurements in the boreal forest and tundra biomes. Climate model simulations indicate that warmth of this magnitude will become the norm by the 2050s if greenhouse gas emissions follow their present scenario.

1. Introduction

Alaska experienced record-setting warmth during the cold season of 2015/16. (The cold season is defined here as October through April, the seven months in which the statewide average temperature is below freezing). During 2015/16 the statewide temperature for October–April exceeded the period-of-record (1925–2016) mean by 4.7°C (8.4°F) and the current 30-yr (1981–2010) climatological ''normal'' by 4.2°C (7.5°F), exceeding the previous record set in 2002/03 by 0.7°C (1.3°F) [National Centers for Environmental Information (NCEI); NCEI (2016)]. Even more remarkable were the temperatures during the second half of the cold season. The January–April statewide average exceeded the period-of-record mean by 6.1°C (10.9°F) and the 1981–2010 climatological mean by 5.4°C (9.7°F). This January–April anomaly represents a departure of 3.97 standard deviations from the current climatological normal. Figure 1 shows the time series of the statewide temperature anomalies, relative to the 1981–2010 means, for the two seasonal timeframes.

This present paper is intended to provide some context for the record warmth of the 2015/16 cold season in Alaska by addressing two questions: 1) Why was Alaska so warm during the past winter? 2) At what point in the future might the cold-season temperatures of 2015/16 become typical? With regard to the first question, candidate explanations include the anomalies of the atmospheric circulation, anomalous temperatures of air advected into Alaska, the effects of the surface state (i.e., snow and sea ice anomalies that impact air temperatures more locally in and around Alaska), and greenhouse warming. Extreme cold-season temperature anomalies in Alaska have been shown to be associated with anomalous atmospheric circulation patterns (Shulski et al. 2010), with a strengthened Aleutian low resulting in warm advection and a weakened Aleutian low associated with

Corresponding author e-mail: John E. Walsh, jwalsh@iarc.uaf.edu

DOI: 10.1175/JCLI-D-16-0473.1

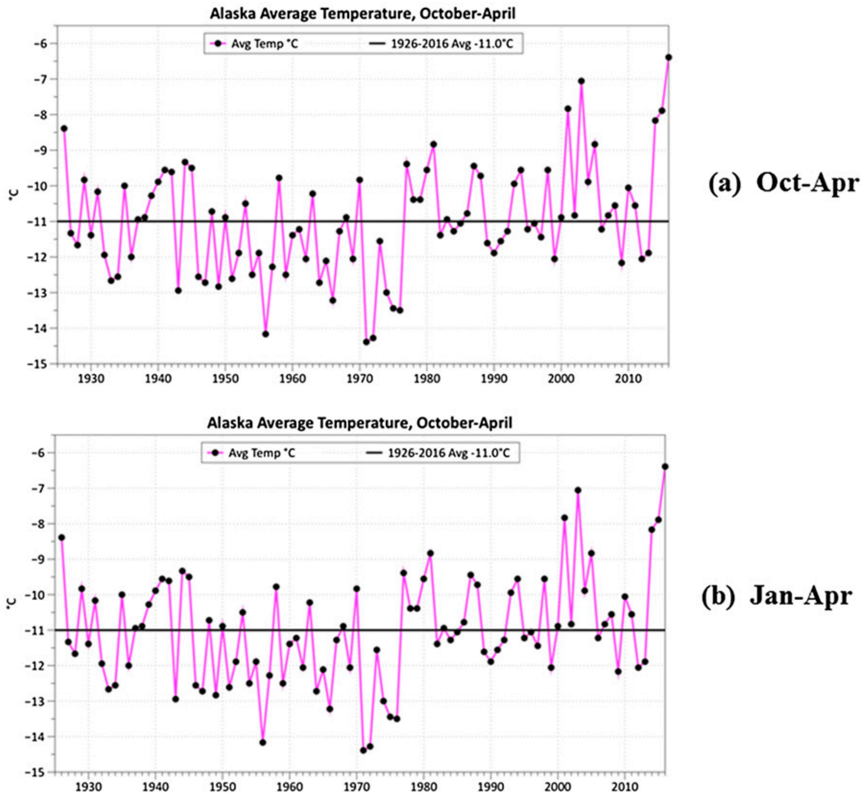

FIG. 1. Alaska statewide average temperatures (°C) for (a) October–April and (b) January–April [data from NCEI (2016)].

cold advection. The atmospheric circulation has also been implicated in the warmth of the broader Arctic during the winter of 2015/16 (Overland and Wang 2016; Cullather et al. 2016). We therefore hypothesize that advection played at least some role in Alaska's anomalous warmth during the 2015/16 cold season. The present paper is intended to determine the magnitude of the circulation's contribution to the warm winter.

The core of the experiments described in the following section is the use of an analog approach that identifies the years with the most similar wind patterns over Alaska, enabling a comparison of the 2015/16 air temperatures with those expected on the basis of the best past analogs of atmospheric circulation. A similar approach has been used in attribution studies for extreme seasons in Europe (Cattiaux et al. 2010; Yiou et al. 2007). We also examine sea surface temperature, sea ice, and snow conditions in the context of the abnormal warmth. With regard to the future expectations raised by the second question above, climate models run under greenhouse gas emission scenarios have provided projections of climate change through 2100. Here we utilize output from global climate models and a regional climate simulation for Alaska, with a focus on the trends and variability of the simulated temperatures over Alaska from the late 1900s through 2100. Extreme warm winter temperatures (by historical standards) become more frequent in future decades in the model simulations, enabling estimates of the future time at which the 2015/16 winter's temperatures become the norm.

2. Methods

The atmospheric circulation exerts a strong control on temperature variations through the advection of warm and cold air across temperature gradients. Extreme cold events in middle latitudes, for example, are associated with the advection of cold air masses from high latitudes. It follows that monthly and seasonal anomalies of temperature are driven, to some extent, by the atmospheric circulation and temperature advection. To assess the impact of the atmospheric circulation on the temperatures over Alaska during the 2015/16 cold season, we utilize a tool for selecting the closest atmospheric circulation analogs to 2015/16 in the historical database. The historical database used here is the NCEP–NCAR reanalysis (R1; Kalnay et al. 1996), which spans the period from 1949 to the present.

Because a reanalysis represents a blend of observations and model output, an important consideration is the performance of the reanalysis over the region of interest. Two recent studies have evaluated reanalysis performance over high latitudes: Lindsay et al. (2014) for the Arctic Ocean and Lader et al. (2016) for Alaska. R1 was one of several reanalyses compared in each study. As expected, the fields for which observations were directly assimilated (i.e., pressure/geopotential height, temperature, and wind) showed better agreement across the models and with observational data than did fields that are computed by the models without direct assimilation (e.g., precipitation and radiative fluxes). For our purposes, the sea level pressure and geopotential height fields are the primary concerns because only those variables are used to identify the best circulation analogs. Lindsay et al.'s (2014, p. 2604) model intercomparison showed that ''sea level pressure fields differed very little, except for the 20CR model.'' This finding contrasts with the Southern Hemisphere, where Hines et al. (2000) showed that temporal heterogeneities in the input data lead to artificial trends in surface pressure over the Southern Ocean and Antarctica. Lindsay et al. (2014) did find that R1 wind speeds tended to be lower than the cross-model median over the Arctic Ocean in winter. However, our analog selection does not use wind, and only a small portion of our analog selection domain is over the Arctic Ocean. Lader et al. (2016) did not include sea level pressure or geopotential height in their evaluation, which focused on temperature and precipitation. While Lader et al.'s (2016) results showed heterogeneities in the R1 fields of precipitation and even temperature over Alaska, the assimilation of pressure, geopotential height, and wind data in this reanalysis gives its large-scale circulation fields more credibility, especially over land areas where station data are available for assimilation.

The analog selection procedure is based on root-mean-square (RMS) differences averaged over a prescribed domain. In this case, we select analogs based on sea level pressure (SLP) and 850-hPa geopotential height over a domain that includes Alaska and the surrounding seas: 50°–75°N, 130°W–180°. The evaluation of differences and the analog selection are performed for individual calendar months of the October–April cold season. For example, the best October circulation analogs are obtained by evaluating the RMS differences between the sea level pressure fields of October 2015 and all other Octobers dating back to 1949. We select the five years with the smallest RMS differences as the five best October SLP analogs. We do the same for the 850-hPa geopotential height fields. We then repeat the procedure for each month from November through April, selecting the five best analog years for SLP and 850-hPa height. For each calendar month and variable (SLP and 850-hPa height), we use area-weighted averages of the surface air temperatures of the Alaska climate divisions (from NCEI), average over the five best analogs, and compare the five-analog average to the corresponding temperatures of 2015/16, thereby determining how much of the 2015/16 temperature anomaly can be explained by the atmospheric circulation in each calendar month. While the circulation (SLP and 850 hPa) analogs are obtained from reanalysis output, all temperatures used in this study are NCEI-computed statewide or regional averages based only on station temperature measurements. Specifically, we use the NCEI temperatures for Alaska climate divisions developed by Bieniek et al. (2012). These climate divisions, shown in Fig. 2, have been used in an evaluation of historical variations and trends of Alaskan temperatures (Bieniek et al. 2014) and were recently adopted for use by NCEI (NCEI 2016).

Figure 3 provides an example of the analog fields, showing the sea level pressure distribution in January 2016 and the five Januaries that were the closest analogs to 2016: 1992, 2001, 1981, 1987, and 1958 (from the smallest RMS difference in 1992 to the fifth smallest in 1958). In all cases, strong flow into Alaska from the southeast is indicated by the isobar patterns. Also, in all cases, the SLP over the Aleutian region was lower than normal, consistent with stronger-than-normal advection of warmer air into Alaska. This airflow pattern is consistent with above-normal temperatures. The statewide temperature averaged over these five Januaries was 4.1°C above the 1981–2010 mean, a large departure when one considers that four of the analog years are included in the 30-yr period used to calculate the mean. When the analogs for January 2016 are computed from 850-hPa geopotential height instead of SLP, the five best analogs are from January 1992, 1958, 1981, 2001, and 1961. The commonality across the two sets (4 out of 5 the same, although with different order) is typical of other calendar months.

The magnitude of the warmth of 2015/16 relative to the analog years is a central result of this study, so it is important to document sensitivities to the method used to select the analogs. The analog-derived temperature anomalies associated with the circulation depend on the choice of variable(s) used in determining the best analogs and on their weighting if more than one variable is used. We illustrate this sensitivity in Fig. 4 and again in section 3. Figure 4 shows the statewide average temperatures (departures from 1925–2015 mean) averaged over the five best analogs based on sea level pressure only and the five best analogs based on a combination of sea level pressure and 850-hPa height (equally

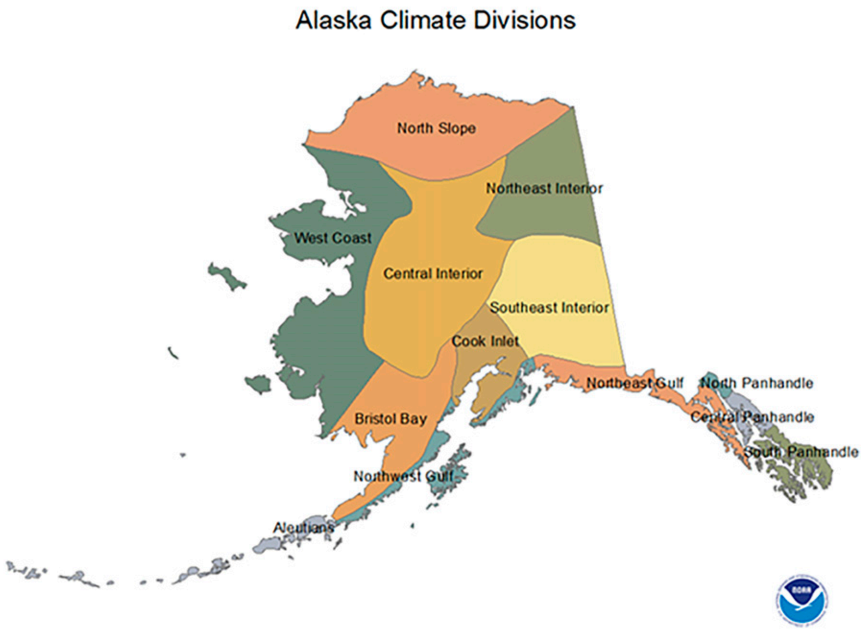

FIG. 2. Alaska climate divisions from NCEI (https://www.ncdc.noaa.gov/file/alaska-climate-divisionspng), based on Bieniek et al. (2012).

weighted). Results are shown for each calendar month, together with the observed temperature anomaly for that month. It is apparent that the inclusion of 850-hPa heights provides no systematic improvement. Our interpretation is that the two fields are largely redundant and that surface air temperature anomalies are most closely aligned with the near-surface winds compared with those 1–2 km above the surface. Experiments with

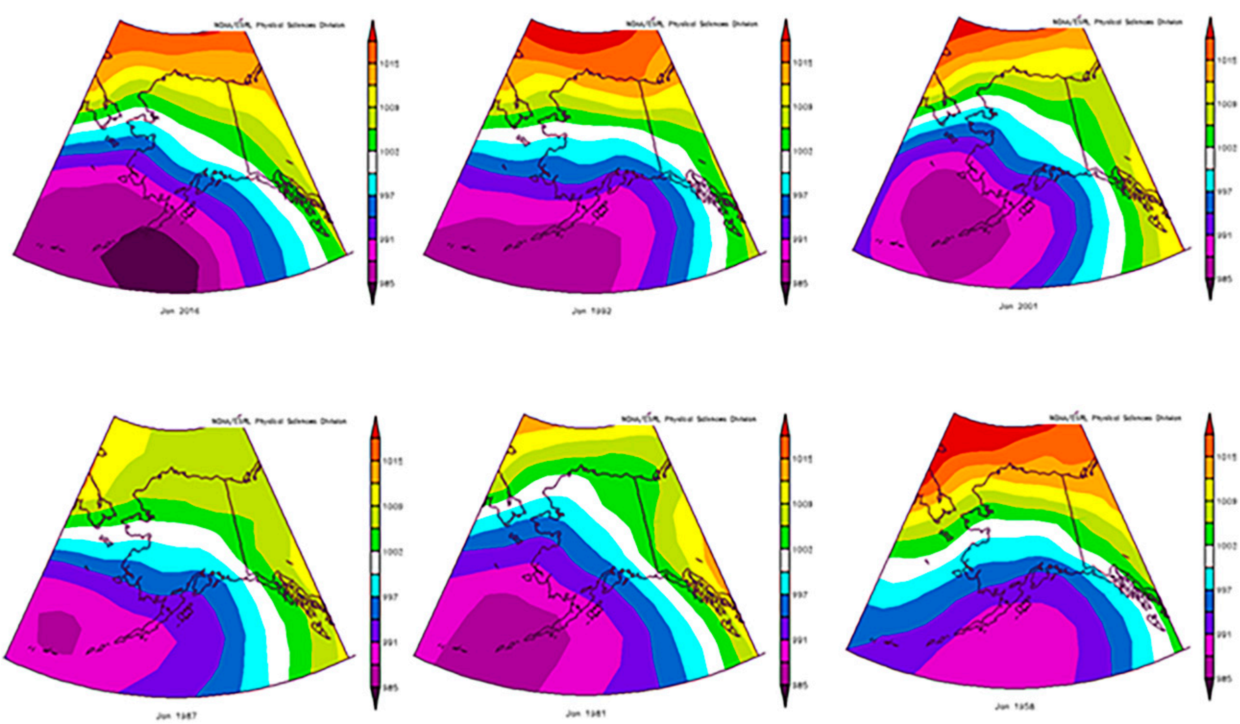

FIG. 3. January SLP (hPa) maps for (top left) 2016 and the five best January SLP analogs: (top center) 1992, (top right) 2001, (bottom left) 1981, (bottom center) 1987, and (bottom right) 1958.

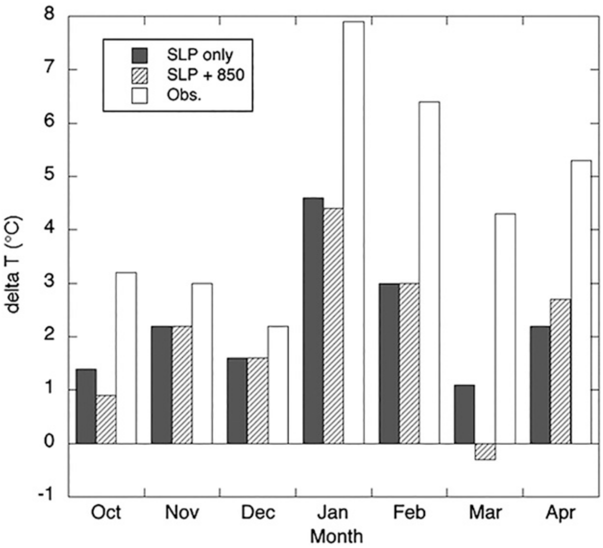

FIG. 4. The statewide temperature anomalies (departures from the 1925–2015 mean) averaged over the five best analogs for 2015/16 based on SLP only (solid bars) and the five best analogs based on an equally weighted combination of SLP and 850-hPa height (hatched bars). Results are shown for each calendar month, together with observed temperature anomalies from 2015/16 (unshaded bars).

different weights of SLP and 850-hPa height did not change this conclusion. In fact, the two sets of analog-derived temperatures are identical in several months because the five best analog years for these months were the same for sea level pressure and 850-hPa height. (Of the 35 selected analogs, 5 in each of the 7 months in Fig. 4, 26 were common to both sets).

Another degree of freedom is the number of selected analogs from which a composite is constructed to evaluate the circulation-driven component of the temperature anomaly. Table 1 shows the mean absolute difference between the analog-derived and observed Alaska statewide-averaged temperature as a function of N, the number of best analog years that are averaged. The results in Table 1 are based on evaluations for each individual month, October through April of 2015/16, and these averages are shown for 1) analogs based only on sea level pressure only and 2) analogs bases on an equal weighting of sea level pressure and 850-hPa geopotential height. It is apparent from Table 1 that the reliance on a single circulation analog is not optimal and that there is little to be gained beyond the use of about five analogs. The initial decrease in error from $N = 1$ implies that the analog procedure has some inherent instability that is offset by the compositing of several analogs, while the lack of improvement beyond $N = 5$ reflects the inclusion of progressively poorer matches of the respective fields.

Finally, we also examined the sensitivities of the analog selection to the spatial domain and to the metric of correspondence. The two metrics of correspondence were the RMS difference and the spatial pattern correlation. The latter was a candidate for the selection of pressure/height analogs because it is the gradients of these variables that determine the winds. Table 2 shows that the differences between the analog-derived and observed statewide average temperatures were similar for the two metrics of correspondence, although the RMS metric resulted in smaller differences (smaller underestimates) in most months and in the 7-month averages. The domain for this comparison (50°–75°N, 130°W–180°) encompasses the state of Alaska, for which the atmospheric circulation and its advective effects are our primary target. When the domain was doubled and quadrupled in size while still centered on the same location, the temperature differences generally worsened, as shown in the lower portion of Table 2.

In view of the results in Fig. 4 and Tables 1 and 2, our use of the analog method to evaluate the circulation-derived component of the temperature anomalies will be based on the use of only sea level pressure, on $N = 5$ analogs, on the RMS metric of agreement, and on the domain bounded by 50°–75°N, 130°W–180°.

TABLE 1. Mean absolute differences between Alaska statewide temperature (°C) of 2015/16 and analog years as a function of the number N of best analogs, where N ranges from 1 (best analog) to 10 (average of 10 best analogs). Results are averaged over analog selections for each month of cold season (from October to April) and are shown for analogs based on SLP only and on equally weighted SLP and 850-hPa geopotential height (SLP + 850 Ht).

	No. of analogs N									
	1	2	3	4	5	6	7	8	9	10
SLP only	3.3	3.0	2.1	2.2	2.3	2.5	2.7	2.7	2.3	2.7
SLP + 850 Ht	3.6	2.4	3.0	2.7	2.5	2.6	2.8	3.0	3.1	3.2

3. Temporal and spatial distributions of the excess warmth

Prior to quantifying the effect of the atmospheric circulation, we first extend the diagnosis of the winter warmth to include the spatial and intraseasonal distributions of the departures from the mean temperature. Because the proximity to surface anomalies (ocean temperature, sea ice, and snow) varies regionally and because the incoming solar radiation has a strong seasonal variation, the spatial and temporal distributions of the temperature anomalies can provide clues to the relative importance of various drivers of the air temperature anomalies over the state.

The abnormal warmth affected all parts of the state, although the magnitudes of the temperature anomalies

TABLE 2. Mean absolute differences between Alaska statewide temperature (°C) of 2015/16 and analog years as a function of metric used in analog selection [RMS difference vs pattern correlation (PC)] and as a function of the domain size (with RMS difference as the metric).

	Oct	Nov	Dec	Jan	Feb	Mar	Apr	Oct–Apr
RMS; 50°–75°N, 130°W–180°	1.7	0.7	0.6	3.3	3.4	3.3	3.1	2.3
PC; 50°–75°N, 130°W–180°	3.1	0.7	0.9	4.2	2.3	4.3	2.6	2.6
RMS; 50°–75°N, 130°W–180°	1.7	0.7	0.6	3.3	3.4	3.3	3.1	2.3
RMS; 45°–80°N, 118°W–168°E	3.1	1.7	1.2	3.3	2.7	3.9	2.6	2.6
RMS; 40°–90°N, 105°W–155°E	3.4	3.3	0.5	5.8	5.9	4.0	2.9	2.9

were largest in the western and central regions. Figure 5 shows the departures from the October–April period-of-record means in each of the state's 13 climate divisions shown in Fig. 2. The 7-month departures from the corresponding divisional means range from 2.4°C in the South Panhandle and 2.5°C in the Aleutians, to 5.3°C in the West Coast and Central Interior divisions and a maximum of 5.9°C in the Bristol Bay division. The North Slope, North Panhandle, and Central Panhandle divisions each recorded the second-highest 7-month departures of their 91-yr records. All other divisions had their largest departures on record. For the latter part of the cold season (January–April), new 4-month records were set in all climate divisions except the North Panhandle, for which 2016 ranked second only to 1926.

The departures from the climatological means were substantially larger in the later months (January–April) than in the early months (October–December) of the cold season. Figure 6 shows this seasonality in terms of calendar-month statewide averages of the divisional anomalies (area weighted) with respect to three climatological base periods: 1925–2016 (the full period of record for the climate divisions), 1949–2016 (the period of R1 used for selecting circulation analogs), and 1981–2010 (the period for the current climatological ''normals'' used by the National Weather Service). For October and November, the departures show essentially no variation among the three choices of base period, indicating that there has been little change in the calendar-month means. However, for December–April, the departures relative to the 1981–2010 means are smaller than the departures relative to the full-period means by 1.5°, 0.6°, 0.8°, 0.8° and 0.6°C, respectively, indicating that the climatological means have increased over time. Despite the change in the means, the monthly departures are positive in all calendar months for all three base periods. The larger departures in January–April compared to October–December are also apparent in all three cases, and the differences between the two subseasons are greater than the differences arising from the choice of the base period.

Figure 7 compares the October–December and January–April departures (relative to the 1925–2016 means) as a function of climate division. The difference between the two seasonal subperiods is large (3°–4°C) over most of the state, ranging up to 4.5°C on the North Slope, where the departures were 1.6°C for October–December and 6.1°C for January–April. The changes from the earlier to the later subperiod are generally smaller in the southern and southeastern coastal climate divisions, although the differences are still generally between 2° and 3°C in those climate divisions.

A key question for this study is as follows: How much of the temperature anomalies documented above resulted from the atmospheric circulation anomalies? We address this by plotting the ''excess warmth,'' defined here as the amount by which the departure from the mean temperature (Figs. 6 and 7) exceeds the composite (mean) of the corresponding departures in the five best circulation-derived analog years. Stated differently, the excess warmth is the portion of the temperature anomaly that cannot be attributed to the atmospheric circulation pattern of 2015/16. Figure 8 shows the statewide average of excess warmth for 2015/16 (relative to the SLP-derived

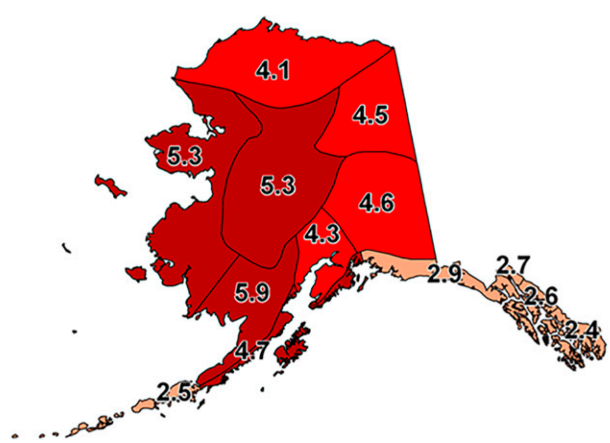

FIG. 5. Departures from the October–April period-of-record (1925–2015) mean temperatures (°C) for the 13 climate divisions of Alaska. Darker shades of red denote larger values.

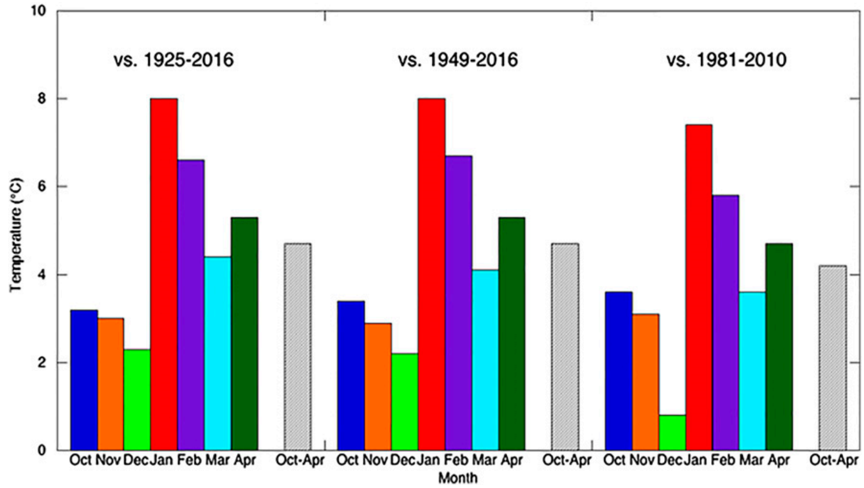

FIG. 6. Calendar-month statewide averages of the 2015/16 anomalies of temperature with respect to three climatological base periods: (left) 1925–2016, (center) 1949–2016, and (right) 1981–2010.

analogs) as a function of calendar month. For the 7-month period as a whole, the statewide average of the excess warmth is 2.4°C, which is 57% of the total anomaly (relative to the 1981–2010 mean). However, the excess warmth and its percentage of the total departure both increase substantially from the early season to the late season: from 1.1°C (45% of the total) for October–December to 3.3°C (69% of the total) for January–April. This seasonal increase has implications for the explanation of the excess warmth, as discussed below.

Additional explanatory clues can be gleaned from the spatial distribution of the excess warmth, shown in Fig. 9 for October–December and January–April. The largest values for October–December are found in the western climate divisions, where the values are generally around 2°C (Fig. 9, left). Values are quite small, 0.5°C or less, in the North Slope division and in the eastern climate divisions, including the Southeast Interior. Such small values indicate that the temperature anomalies in these divisions during October–December were essentially circulation driven. During these months the excess warmth generally represents larger percentages of the anomalies in the southwestern divisions: Aleutians (97%), Northwest Gulf of Alaska (73%), Cook Inlet (67%), and West Coast (66%). The percentages are smaller in the northern and eastern divisions, ranging down to 0% in the Southeast Interior and the Northeast Gulf of Alaska. The overall area-weighted statewide average of the excess warmth as a percentage of the total departure from the mean is 45%, indicating that slightly more than half of the departure from normal temperature during October–December is explained by the atmospheric circulation.

The excess warmth is considerably greater in the later months, January–April (Fig. 9, right). The excess

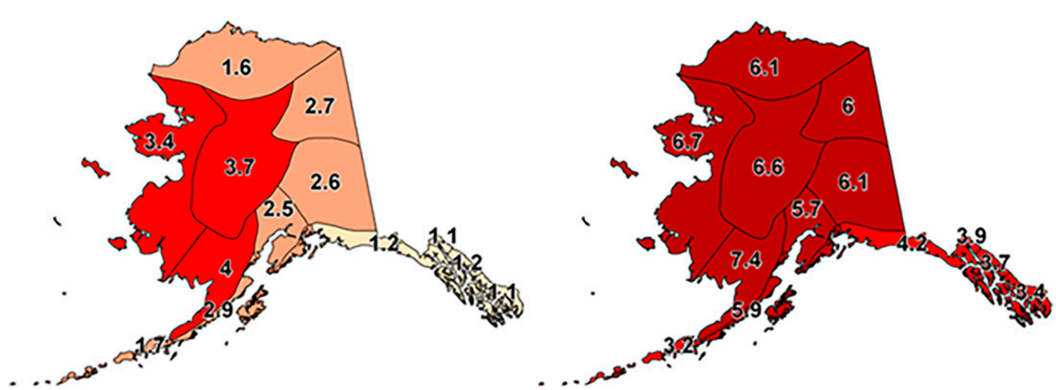

FIG. 7. (left) October–December and (right) January–April departures of temperature (°C) relative to 1925–2016 means for each climate division.

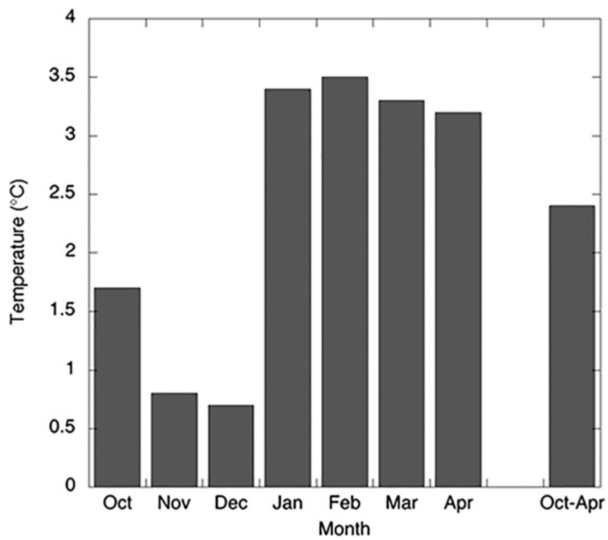

FIG. 8. Statewide average of excess warmth for 2015/16 (°C) as a function of calendar month.

warmth exceeds 3.0°C in the western two-thirds of the state (except for the Aleutians), and it is as large as 4.4°C in the North Slope climate division. Even the smallest values, which are found in the Southeast Interior, are greater than 1.0°C during January–April. Not only are the values of excess warmth larger in January–April than in October–December, but they represent larger percentages of the total anomalies during January–April. The percentages for January–April are 39% or greater in all divisions, and they exceed 60% in six divisions: Cook Inlet (61%), Bristol Bay (62%), West Coast (67%), Northwest Gulf (68%), North Slope (83%), and the Aleutians (93%). For the (area weighted) statewide averages, the excess warmth represents 61% of the total temperature departure during January–April—a considerably larger percentage than the 45% for October–December. We conclude that, unlike the October–December period, the atmospheric circulation accounts for considerably less than half the excess warmth of the January–April portion of the cold season.

4. Other drivers

Interest and activity in extreme event attribution has accelerated over the past decade. Formal attribution analyses have followed most extreme weather and climate events, with the European heat wave of 2003 serving as a seminal event for attribution analysis (Stott et al. 2004). Among the other events that have been the subject of formal attribution analyses are cold outbreaks in the United Kingdom and the United States (Christidis and Stott 2012; Van Oldenborgh et al. 2015; Wolter et al. 2015); flooding events in western Europe and the United States (Otto et al. 2015; Hoerling et al. 2014); drought in Texas and the western United States (Hoerling et al. 2013; Seager et al. 2015); and the Russian heat wave of 2010 (Otto et al. 2012). Summaries and recommended approaches to formal attribution studies have been provided by Hegerl et al. (2007), Trenberth et al. (2015), and Shepherd (2016). Attribution studies generally follow one of two approaches: 1) statistical analyses of observational data, with a focus on the role of climate change in changing the probabilities of threshold exceedances or other characteristics of extreme events and 2) model-based studies in which changes in likelihoods or intensities are based on simulations of a control (counterfactual) climate, the present climate, and, in some cases, future climate (National Academies 2016).

While the present study is not a formal attribution analysis, it is a step toward an attribution study of the extreme temperatures of the 7-month cold season of 2015/16 in Alaska. Specifically, we have quantified in section 3 the role of the atmospheric circulation as one contribution to the extreme temperatures. In this

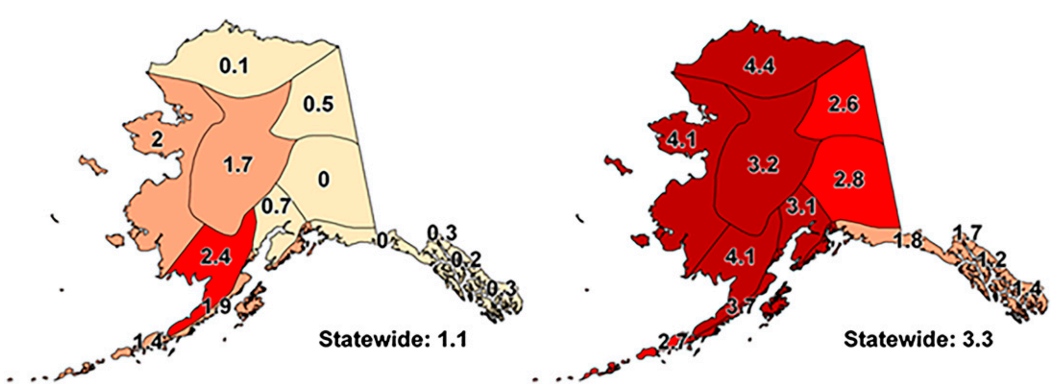

FIG. 9. Excess warmth (defined in text; °C) for (left) October–December and (right) January–April for each climate division. Darker reds denote larger values.

section, we document anomalies that are also likely contributors to the extreme temperatures of the 2015/16 cold season. We do not evaluate these contributions quantitatively because they are intertwined. For example, abnormally warm sea surface temperatures and reduced sea ice and snow cover will be shown to be consistent with the spatial and seasonal patterns of the excess warmth, but variations of these quantities are inseparable from greenhouse gas forcing, another contributor to the warm temperatures. For example, greenhouse warming has almost certainly contributed to the recent reduction of Arctic sea ice cover (Notz and Marotzke 2012; IPCC 2013) and most likely to the reduction of snow cover on land (Derksen and Brown 2012). Even the atmospheric circulation may be impacted by increasing greenhouse gas concentrations, although such associations are poorly documented, primarily because any such greenhouse warming–circulation relationships are obscured by internal variability (Shepherd 2014).

Section 3 identified spatial and intraseasonal patterns in the excess warmth, including the portions of the temperature anomalies that can be explained by the corresponding anomalies of the atmospheric circulation. For the entire 7-month period, more than half (57%) of the positive departures from the climatological mean temperatures cannot be explained by the atmospheric circulation. The fraction that cannot be attributed to the atmospheric circulation is largest in the second portion (January–April) of the cold season. As possible explanations for the excess warmth, we identify three candidate mechanisms:

(i) excess warmth of the air advected into Alaska because of passage over abnormally warm surfaces (high sea surface temperatures and absence of sea ice);
(ii) surface energy budget perturbations arising from a deficient snowpack over the land area of Alaska; and
(iii) increased greenhouse gas concentrations and associated increases in downwelling longwave radiation.

While these three mechanisms involve distinctive processes and have different signatures, they are not independent. For example, greenhouse gas–driven warming may reduce snow cover and sea ice, or it may contribute to heating of the upper ocean (sea surface temperatures).

The 2015/16 cold season occurred during a strong El Niño. El Niño occurrences are known to affect temperatures in Alaska (Papineau 2001). In addition, the Pacific decadal oscillation (PDO) index was strongly positive during the October–April period of 2015/16. The PDO has also been shown to influence Alaska winter temperatures (Hartmann and Wendler 2005; Mills and Walsh 2013), although with a signature that is nonstationary in time (McAfee 2014). During the October–April period of 2015/16, the multivariate El Niño index (MEI) and the PDO index were both the third highest of the post-1949 period. However, El Niño and PDO influences can be placed into two categories: 1) impacts on the atmospheric circulation, which are already built into our evaluation of excess warmth through the use of best circulation analogs, and 2) ocean temperature (and possibly sea ice) anomalies, which are also incorporated into our assessment framework (i) above. Moreover, as shown in Table 3, the Alaskan temperature anomalies in other strong El Niño and PDO years of the post-1949 period were much smaller than in 2015/16, averaging 0.3°C over the cold seasons of the eight other strongest El Niño years and 1.6°–1.7°C over the eight other strongest PDO years. We conclude that the magnitude of the warmth of the 2015/16 cold season in Alaska cannot simply be attributed to El Niño and the PDO.

a. Abnormal warmth of air advected into Alaska

As in most regions, Alaska's temperatures vary with airmass advection in addition to the seasonal cycle. Winds from the south generally bring temperatures warmer than the seasonal normal, while winds from the north generally bring colder-than-normal temperatures. This impact of advection should be captured by the atmospheric circulation (SLP or 850 hPa) analogs, and it indeed was, according to the analog-derived composite temperatures. In all months of the 2015/16 cold season, the temperature anomalies of the analog years were above the climatological means, especially during the second half of the cold season. However, the analog-derived temperatures were not as warm as observed, with discrepancies typically 2°–3°C in October–December and 4°–7°C in January–April. Was this because the air advected into Alaska was warmer than it was during the analog years? Figure 10, which shows midwinter sea surface temperature anomalies, suggests that the answer is ''yes, to a limited extent.'' Sea surface temperatures to the south and west of Alaska were 0.5°–1.5°C above normal and above the analog-year means, meaning that low-level airflow from the south and southeast (the prevailing wind directions implied by Fig. 3) should have been warmer than normal by comparable amounts. The relatively warm sea surface temperatures were remnants of the ''blob'' of anomalously warm surface water that had been present for about two years in the North Pacific Ocean south of Alaska (Bond et al. 2015). Further evidence is provided by Fig. 11,

TABLE 3. Alaska statewide temperature anomalies ΔT (°C) during years in which the October–April MEI and the PDO index had their highest values (>1.0) during the post-1949 period.

MEI	Year	ΔT (Oct–Apr)	ΔT (Jan–Apr)	PDO	Year	ΔT (Oct–Apr)	ΔT (Jan–Apr)
2.7	1983	0.1	0.4	1.8	2015	3.1	2.9
2.6	1998	1.4	2.6	1.8	1987	1.6	1.3
2.1	2016	4.6	6.0	1.7	2016	4.6	6.0
1.7	1992	−0.3	−0.1	1.4	1984	−0.3	−1.4
1.4	1987	1.6	1.3	1.4	2003	3.9	3.1
1.3	1958	1.2	1.7	1.3	1998	1.4	2.6
1.3	1966	−2.2	−2.6	1.2	1988	1.3	1.7
1.3	1973	−0.6	−1.5	1.1	1994	1.4	0.4
1.2	2010	0.9	0.8	1.0	1977	1.6	1.8
Mean ΔT (2016 excluded)		0.3	0.3			1.7	1.6

which shows the sea ice coverage as departures from the climatological mean ice concentrations for November and January. (Departures from the analog-year means for these months show little difference from Fig. 11 because the mean ice cover of the analog years was close to the climatology.) The 2016 maximum Bering Sea ice coverage (reached in late March) was the second lowest in the satellite record, which dates back to 1979. Figure 11 shows that considerably more open water was present during early winter (November) and in midwinter (January) than in the corresponding climatological means. Air advected into Alaska from the west and southwest in 2016 would be expected to be warmer than in the past because of greater exposure to open water in the Bering Sea.

While the distributions of sea surface temperature and sea ice favor above-normal temperatures, they cannot account for the large anomalies that were observed. The broader distribution of winter temperatures (Fig. 12) provides an example. The surface air temperature departures (from the 1981–2010 means) were far larger over Alaska than over the surrounding ocean. It is apparent that ocean temperatures and sea ice coverage alone contributed to, but cannot explain the full magnitude of, Alaska's temperature anomalies during the 2015/16 cold season.

b. *Deficiency of snow*

The 2015/16 cold season was marked by abnormally sparse snow cover in Alaska. While significant early-season snows occurred in September in northern and central Alaska, much of this snow melted before the "permanent" winter snowpack was established. November snowfall was generally above normal, but snowfall was far below normal from December onward. The statewide average snowfall was 70% of normal in December and January, 20% of normal in February, 45% of normal in March, and 33% of normal in April (Alaska Climate Research Center 2016). Figure 13 shows the percentage of normal snow depths on 1 March at the first-order reporting stations in Alaska. The vast majority of the stations reported large snow deficits, especially in the southern parts of the state, where snow depths at many locations were less than 25% of normal. In the Interior, the snow depths were

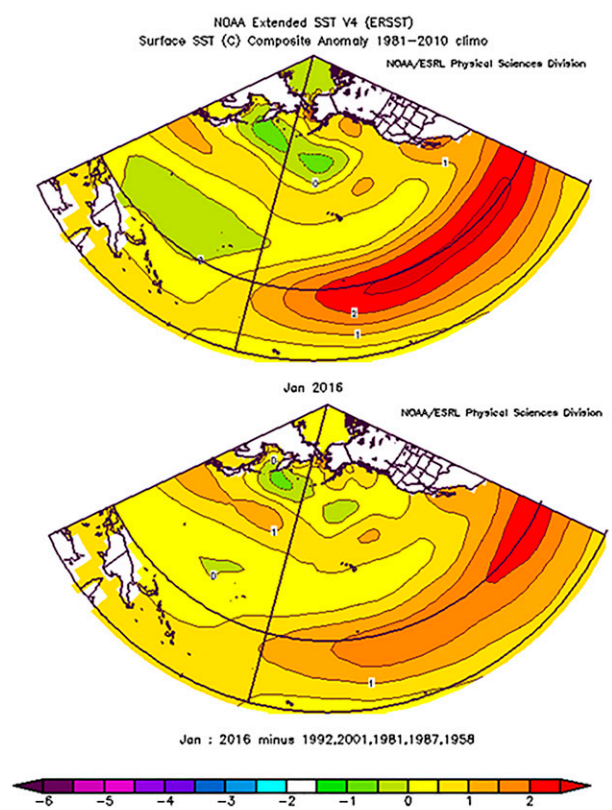

FIG. 10. Sea surface temperature anomalies (°C) in January 2016 (top) relative to means for 1981–2010 and (bottom) relative to the mean for the five best analog years. (Source: NCEP–NCAR reanalysis; map produced using software of NOAA/Earth System Research Laboratory, https://www.esrl.noaa.gov/psd/cgi-bin/data/composites/printpage.pl.).

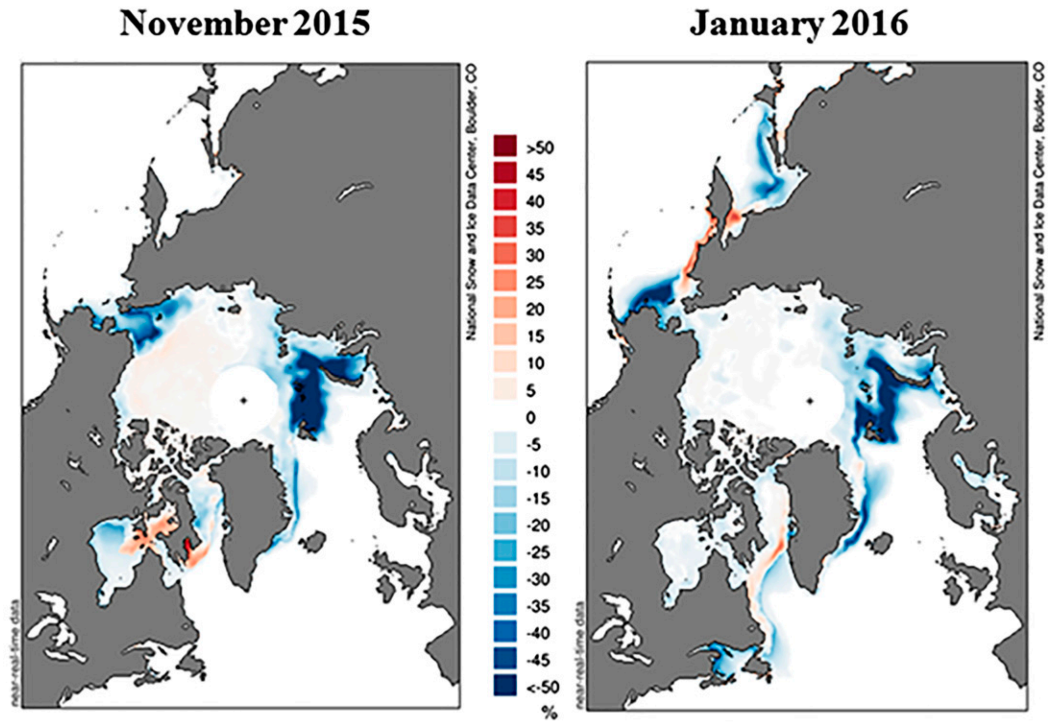

FIG. 11. Sea ice concentration as departures from 1981–2010 monthly means for (top) November 2015 and (bottom) January 2016. Passive microwave sea ice data described by Meier et al. (2014). (Source: National Snow and Ice Data Center, University of Colorado; https://nsidc.org/data/seaice_index/more-about-monthly.html).

generally below normal by up to 50%. Because the first-order stations are primarily located in low-elevation areas, such as river valleys, we also examined the SNOTEL reports that are generally obtained from higher-elevation sites. Our synthesis included all SNOTEL sites with at least five years of data, thereby allowing comparisons with at least minimal climatologies. Table 4 shows that the percentage of SNOTEL sites reporting snow depths less than their climatological means ranged from 60% on 1 March to 81% on 1 May. The median anomalies ranged from −7% on 1 March to −41% on 1 May. Perhaps more importantly, the average date of snow disappearance in 2016 was 12 days earlier than normal. At only 4 of the 42 sites with complete daily data was the final snow-off date later than the climatological mean date. Snowmelt also occurred abnormally early at the first-order weather stations. For example, Fairbanks in the Southeast Interior climate division lost its snowpack on 8 April, the third earliest date in the record extending back to 1930. Anchorage, in the Cook Inlet climate division, hardly had any snowpack to lose, making the date of snowpack loss nearly meaningless.

Further evidence of a deficient snowpack is provided by the snow cover extent data from Rutgers University's Global Snow Laboratory (Estilow et al. 2015; http://climate.rutgers.edu/snowcover/index.php), which shows that Alaska's March–May 2016 snow cover extent of $1.15 \times 10^6\,km^2$ was the smallest of the 50-yr period of record (1967–2016). The low snow depths and extent, together with warmer-than-normal temperatures, favored an early snow disappearance.

Snow cover can impact surface temperatures, primarily through albedo effects, which are strongest in the late winter and spring. Such impacts have been documented in air temperatures over the contiguous United States (Namias 1985; Walsh and Ross 1988; Mote 2008), over Siberia (Cohen et al. 2001; Alexander and Gong 2011), and over northern high-latitude ecosystems (Euskirchen et al. 2007). The deficient snowpack is implicated in the anomalous temperatures of the 2015/16 cold season by the spatial and seasonal patterns of the excess warmth. First, the excess warmth documented in section 3 (Fig. 8) was much larger in the late winter (January–April) than in the early part of the cold season (October–April). This seasonality is consistent with the available insolation that is subjected to the surface albedo effect, as shown by Euskirchen et al. (2007, their Fig. 5).

As noted earlier, the snow deficiency of 2015/16 did not develop until December, and it became increasingly severe through April. The spatial distribution of the excess warmth is consistent with the expected impacts of the snow deficiency (Fig. 13), especially in

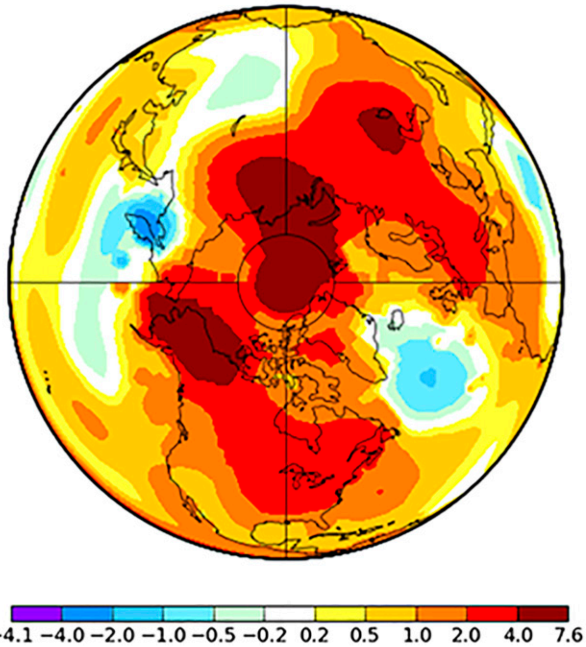

FIG. 12. Temperatures of December–February 2015/16 as departures from the climatological means for 1981–2010. [Source: NASA Goddard Institute for Space Studies (GISTEMP Team 2017; Hansen et al. 2010).]

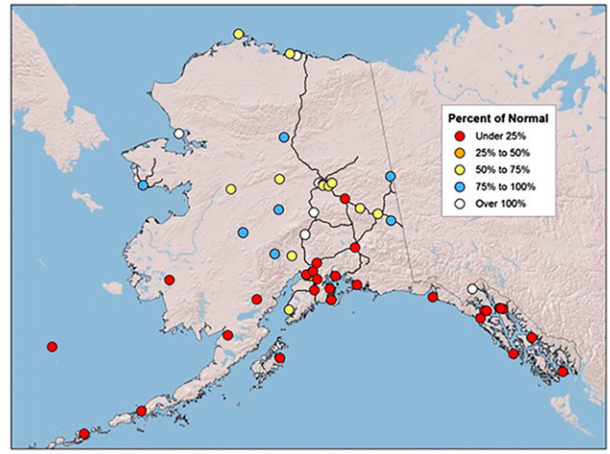

FIG. 13. Percentage of normal snow depth at Alaskan reporting stations on 1 Mar 2016. [Data source: Global Historical Climate Network–Daily, version 3 (Menne et al. 2012a,b), and NOAA/National Centers for Environmental Information.]

January–April. The temperature excesses were largest (>3°C) in the Bristol Bay, Cook Inlet, Northwest Gulf, Central Interior, and West Coast climate divisions (Fig. 9, right), which are areas in which the snowpack deficiency was large and the loss of snow occurred abnormally early. Figure 14 shows that the April surface albedo was significantly lower than in any year for which measurements are available from both the tundra of the North Slope (2008–16) and the boreal forest of the Southeast Interior (2011–16). The lower values at the boreal site are indicative of the earlier snowmelt, which occurred approximately two weeks earlier than the normal snow-off date in the second half of April. At the tundra site, where snow persisted through the month, the lower albedo is consistent with an earlier onset of melt, which tends to darken the surface, and with the generally deficient tundra snowpack indicated in Fig. 13. In the absence of fresh snow, a snow surface will darken over time. Another factor that reduces the albedo when there is a deficit of snow is the exposure of vegetation. In the shrub tundra environment of Fig. 14a and especially the boreal landscape of Fig. 14b, vegetation darkens the surface and accelerates the melt of snow during spring. Figure 15 (top) shows the dark patches within the degrading snowpack of the boreal forest in April at a Long-Term Ecological Research (LTER) site (Bonanza Creek) in the Southeast Interior climate division.

Within the January–April period, the excess warmth was about as large in January and February as in the later months (Fig. 8). For this particular winter, the vegetative masking effect may have played a role even before the late-season melt began, especially in the boreal forest. Because long periods during December–February had no new snowfall to replenish the snow and rime that had blown off the trees during occasional wind events, the boreal landscape was considerably darker than usual in midwinter (Fig. 15, bottom). However, the incoming solar radiation is small enough within a month or so of the winter solstice that this effect is unlikely to have been a major contributor to the excess warmth during January.

There are two additional pieces of evidence for a local influence of snow cover and its albedo effect on Alaska temperatures of 2016. The first is the fact that the temperature anomalies were larger over Alaska than over the surrounding oceans (Fig. 12). The second is the spatial distribution of excess warmth for May 2016. May is not included in our primary analysis because it is not a ''cold season'' month. With a statewide mean temperature of about 3°C, May is Alaska's ''spring'' month. At

TABLE 4. Summary of snow depth anomalies during spring 2016 at SNOTEL sites in Alaska. Number of reporting SNOTEL sites ranged from 42 in March to 46 in May.

	SNOTEL stations with below-normal snow depth	Median snow depth anomaly
1 Mar	60%	−7%
1 Apr	69%	−26%
1 May	86%	−41%

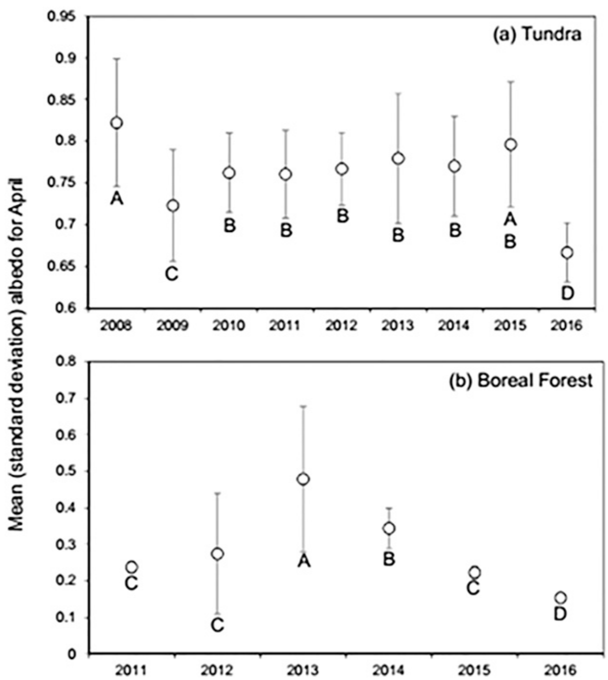

FIG. 14. Monthly mean surface albedo for April based on radiative flux measurements at (a) a tundra site, Imnavait Creek (68.6°N, 149.3°W) in the North Slope climate division, and (b) a boreal forest site, Bonanza Creek (64.7°N, 148.3°W) in the Southeast Interior climate division. Letters are based on a Duncan's multiple range test to show significant differences between the monthly means. April 2016 had significantly lower albedo than any of the other measured years in both the tundra and boreal forest.

the start of May, much of the northern half of the state is still generally snow covered, while the snow is typically gone by the end of May except for the North Slope. The North Slope's snow typically melts rapidly in late May and early June. May is also the month in which much of the sea ice cover south of the Bering Strait melts, while the ice cover north of the Bering Strait persists into June (as it did in 2016). Figure 16 shows that the excess warmth in May was largest in precisely the areas that are the last to lose their snowpack in most years: the North Slope and the West Coast. The excess warmth in these two divisions was 5.3° and 5.1°C, respectively, among the largest of all division/months. Values in the state's southern divisions, which are typically snow free during May in all years (except for higher terrain), are much smaller. Because the loss of the snowpack occurred during May but earlier than usual in the northern division, while there were no negative snow anomalies in the south, the pattern in Fig. 16 is consistent with the signature of early snow loss, which was foreshadowed by the abnormally low April surface albedos measured over North Slope tundra (Fig. 14a). An early loss of sea ice likely also contributed to the large temperature excess along the West Coast, especially in the Norton Sound region south of the Bering Strait.

c. *Increasing greenhouse gas concentrations*

An additional consideration in the assessment of the anomalous warmth of 2015/16 is the increase of greenhouse gas concentrations and associated radiative forcing. Here, a key consideration is the gradual nature of the increase of greenhouse gas concentrations. CO_2 concentrations, for example, have increased from approximately 350 ppm in 1990 to about 400 ppm in 2016. NOAA's annual greenhouse gas index (AGGI; Hoffmann et al. 2006; http://esrl.noaa.gov/gmd/aggi/), which includes effects of other increased greenhouse gases in addition to CO_2, has increased by about 40% since 1990. Global climate models run under greenhouse gas forcing scenarios project a warming of Alaska by 5°–9°C (Melillo et al. 2014) over the 100 years from 1971–2000 to 2071–99. The warming rate is subject to uncertainties arising from the emission scenario, cross-model differences in formulation, and internal variability. Hodson et al. (2013) place these uncertainties into a framework of warming for the Arctic. For the Alaska region, Fig. 17 provides an example of simulated temperatures from the CMIP5 model ensemble (36 models) depicting uncertainties due to internal variability (the short-term variations in Fig. 17) and cross-model differences (the gray shades in Fig. 17) in simulations forced by the representative concentration pathway 8.5 (RCP8.5) scenario. The cross-model mean (red line in Fig. 17) averages out much of the internal variability as well as the cross-model differences, leaving primarily the effect of external forcing, which is primarily the greenhouse gas signal modified by aerosol effects. The average warming of the cross-model mean over the several decades centered on 2015 is approximately 2°C $(30\,\mathrm{yr})^{-1}$, or about 0.6°–0.7°C decade^{-1}. The corresponding rate under the representative concentration pathway 4.5 (RCP4.5) scenario is slightly smaller. These simulations use historical forcing through 2005 and the RCP forcing thereafter; the RCP scenarios do not show a large divergence in the Arctic until about midcentury (Overland et al. 2014).

At a warming rate of 0.6°–0.7°C decade^{-1}, and ignoring internal variability, 2015/16 would be warmer than the 1981–2010 mean by slightly more than 1°C. Consistent with the preceding discussion, this estimate represents a greenhouse warming signal averaged over all the models in Fig. 17. Some models have stronger warming and others weaker warming, and the warming rates are correlated with the rates of sea ice loss. In particular, the

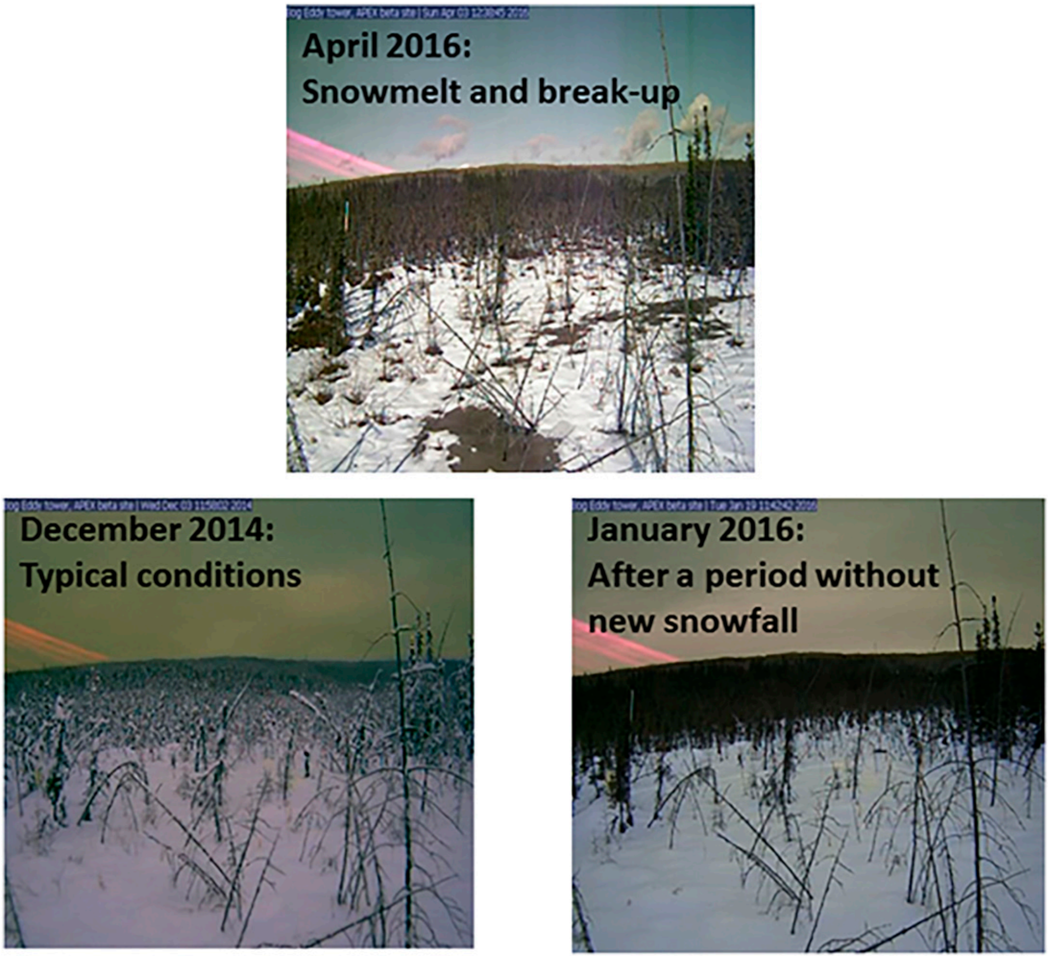

FIG. 15. Tower webcam images from Bonanza Creek LTER site in the boreal forest. (top) The surface during the snowmelt period of April 2016. (bottom) Midwinter images from (left) December 2014 and (right) January 2016. The absence of snow and rime on the trees in January 2016 results in a noticeably darker landscape than in December 2014.

warming is greatest in those models that lose the most sea ice (Rosenblum and Eisenman 2016, their Figs. 4, 5; Stroeve and Notz 2015, their Fig. 1). Various studies have also shown that the recently observed loss of sea ice exceeds that in the historical simulations by most global climate models (Stroeve et al. 2012; Rosenblum and Eisenman 2016) and that the models' sea ice is less sensitive to global temperatures than is observed sea ice (Stroeve and Notz 2016; Rosenblum and Eisenman 2016). It has also become apparent that anthropogenic warming has contributed to the recent observed sea ice loss (Notz and Marotzke 2012; IPCC 2013). For these reasons, one cannot dismiss the possibility that 1°C is an underestimate of the greenhouse gas contribution to the warmth of the 2015/16 winter in Alaska. With this caveat, however, the greenhouse warming contribution of 1°C is far less than the temperature anomalies Alaska experienced during the 2015/16 cold season, pointing to the importance of interannual variability driven by the atmospheric circulation and leveraged by the surface boundary conditions discussed in (i) and (ii) previously. While the surface boundary conditions may be influenced by greenhouse warming, the overall rate of greenhouse warming is too slow to explain the abnormal warmth of 2015/16. A season like 2015/16 may indeed be more likely than in the past, when its observationally derived probability was essentially zero, but factors other than greenhouse warming were clearly at work in 2015/16. With the warming trends projected by climate models, the probability of a warm winter like 2015/16 will increase, becoming approximately 50% at the time when the future warming is equal to the 2015/16 temperature departures of +4.2°C (October–April) and +5.4°C (January–April) relative to the 1981–2010 means. In the

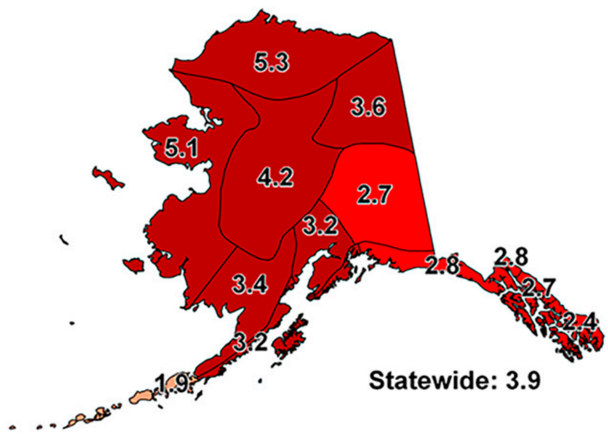

FIG. 16. Excess warmth (portion of temperature anomaly not explained by atmospheric circulation; °C) in each Alaska climate division during May 2016.

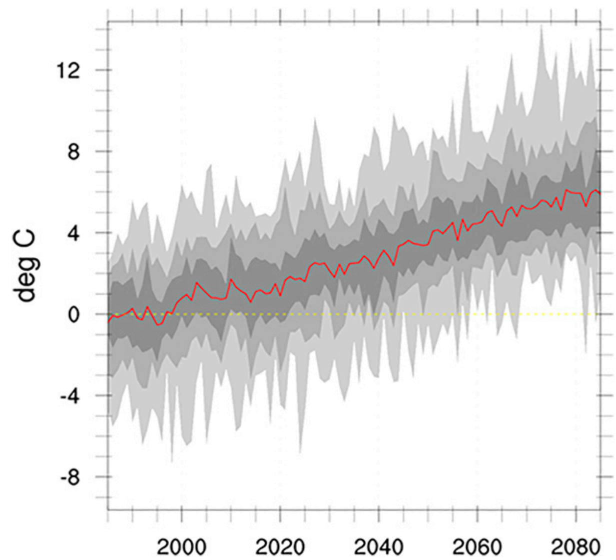

FIG. 17. January surface air temperatures over the eastern Bering Sea simulated by the ensemble of 36 CMIP5 models. Red line is 36-member ensemble mean; light shading denotes range of all models; medium shading denotes range of 80% of models (10th–90th percentiles); dark shading denotes range of 50% of models (25th–75th percentiles). [Source: NOAA/Earth System Research Laboratory; http://www.esrl.noaa.gov/psd/ipcc/cmip5/ (Scott et al. 2016).]

following section, we address the time scale over which this change in probability may be expected to occur.

5. Anticipation of the future

The fact that greenhouse gas–driven temperature changes are consistent in sign, but too small in magnitude, to explain the warmth of the 2015/16 cold season raises an intriguing question: At what point in the future will the warmth of 2015/16 become the norm in Alaska? In other words, if the winter temperatures of 2015/16 were a preview of Alaska's future, what is the timeframe that was previewed? To address this question, we utilize several sources of output from climate models run under future emission scenarios. The emission scenarios on which we focus (SRES A2 and RCP8.5) are those that most closely track the current trajectory of emissions and CO_2 concentrations. We utilize three sources of climate model output, each of which allows a determination of when the change from the 1981–2010 statewide mean temperatures reach the values observed in 2015/16: +4.2°C for the April–October average and +5.4°C for the January–April average.

The first source is the suite of 15 CMIP3 models used as input to the *Third U.S. National Climate Assessment* (Melillo et al. 2014). This evaluation was based on A2 scenario simulations reported by Stewart et al. (2013), who analyzed output for three 30-yr time slices of the twenty-first century. Linear interpolation of these 30-yr temperature changes [from Fig. 10 of Stewart et al. (2013)] gives the following years for which the 15-model mean Alaska statewide warming from the late twentieth century exceeds the values observed in 2015/16: 2051 for October–April (warming of 4.2°C) and 2058 for January–April (warming of 5.4°C). These estimates are based on the ensemble means of the models' changes from their respective means for 1981–2010. As in the preceding section, the use of the ensemble means removes much of the internal variability and the cross-model differences. As a result, this approach does not permit quantitative estimates of the changes in the probability of threshold exceedances between the late 1900s and the 2050s. One may reasonably assume that the probabilities increase from near zero to 50% over this timeframe.

The second source is the suite of 36 CMIP5 model simulations. Figure 18 shows the projected warming for the 2010s from these simulations for two forcing scenarios, RCP4.5 and RCP8.5. Figure 18 also illustrates the cross-model differences by showing the results for the 25th-, 50th-, and 75th-percentile models when ranked from the smallest to largest pan-Arctic warming. The Alaska statewide average warming for the mid-2050s ranges from 2.5°C for the RCP4.5 25th percentile to 6.7°C for the RCP8.5 75th percentile. The 50th-percentile values are +3.8° and 5.5°C for RCP4.5 and RCP8.5, respectively. Note that the warming in this case is for the Alaska statewide average land temperatures, which increase somewhat faster than the temperatures over the adjacent seas (e.g., Fig. 17). For the median (50th percentile) models, the +4.2°C threshold of October–April 2015/16 is reached by 2058 (RCP4.5) and

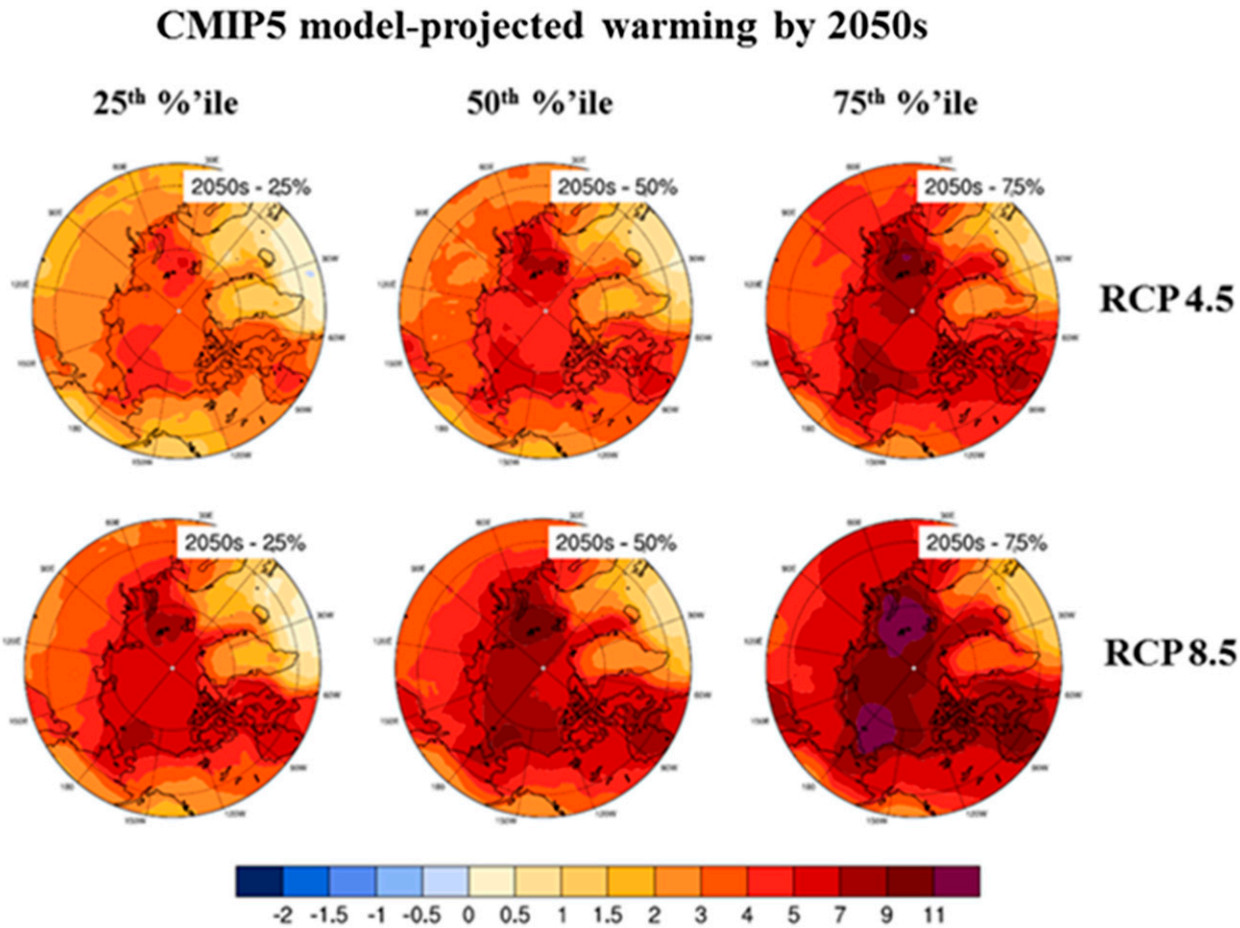

FIG. 18. Patterns of warming projected for the Arctic by CMIP5 models under two forcing scenarios: (top) RCP4.5 and (bottom) RCP8.5. Patterns are shown for (left) 25th-, (center) 50th-, and (right) 75th-percentile models ranked from coldest to warmest on basis of pan-Arctic temperatures. (Figure provided by G. Flato and R. Rong, Canadian Centre for Climate Modelling and Analysis.)

2044 (RCP8.5). The 5.4°C warming of January–April 2015/16 is reached in 2062 (RCP4.5) and 2054 (RCP8.5). The thresholds are reached 5–15 yr later (earlier) if one bases the estimates on the 25th- (75th-) percentile models rather than on the median model.

The third source of future information is a regional climate model simulation performed with the Weather Research and Forecasting (WRF) Model covering the Alaskan domain (Bieniek et al. 2016) and forced at the lateral boundaries by the GFDL CM3 global climate model. We include this single simulation because it preserves the interannual (and other internal) variability that is one of the sources of uncertainty in future projections. In response to the concern that CMIP5 models generally underestimate the recent sea ice retreat and, more generally, the sensitivity of sea ice to global temperature (Stroeve and Notz 2016; Rosenblum and Eisenman 2016), we utilize this model because its future sea ice loss is among the most rapid of the CMIP5 models. The GFDL CM3 also ranks highly among CMIP5 models in its ability to capture recent trends and coverage of Arctic sea ice (Laliberté et al. 2016). The regional model forced by GFDL CM3 was run at 20-km resolution for the period 1970–2100, with observed greenhouse gases through 2005 and the RCP8.5 forcing scenario after 2005. The Alaska statewide temperature anomalies relative to the model's 1981–2010 climatology are shown in Fig. 19. Because of interannual variability, our metric for threshold exceedance was the median temperature of successive 11-yr periods (i.e., 2010–20, 2011–21, … , 2090–2100). The years in which the model's greenhouse warming exceeds the observed anomalies of 2015/16 are 2040 for October–April (warming of 4.2°C) and 2046 for January–April (warming of 5.4°C). The probabilities of an October–April temperature as high as 2015/16 increase from 5% in 2011–30 to 50% in 2031–50 and to 90% in 2051–70. The corresponding probabilities for January–April are 0%, 35%, and 80%.

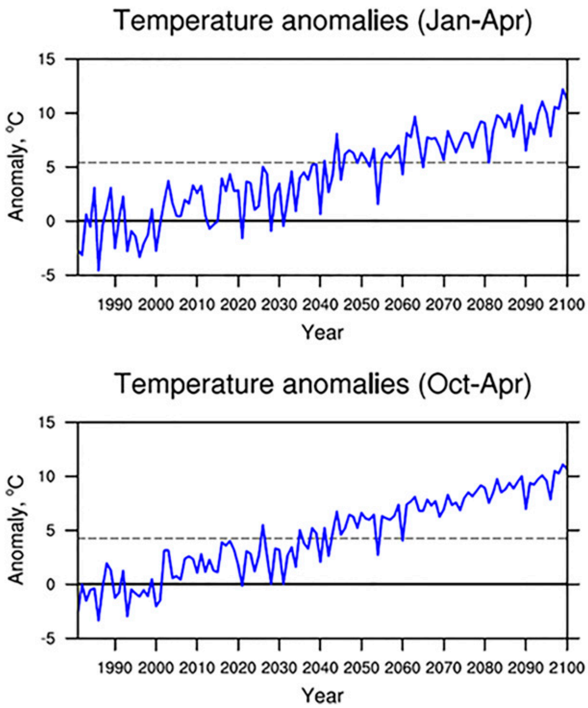

FIG. 19. Time series of Alaska statewide temperatures simulated by WRF regional climate model driven by GFDL CM3 global climate model output under RCP8.5 forcing scenario. Temperatures are plotted as departures from 1981–2010 model means for (top) January–April and (bottom) October–April. Horizontal dashed lines are observed anomalies of 2015/16.

The three sources of model output provide consistent estimates of the timeframe in which the 2015/16 anomalies will become the norm: 2040–50 for the October–April anomaly and 2045–60 for the January–April anomaly. Our conclusion is that, if the models and emission scenarios are realistic, the cold season of 2015/16 will become the norm for Alaska around the middle of the century. In this respect, the 2015/16 cold season was ''ahead of its time'' by three and a half decades.

6. Conclusions

An important issue in this study is the extent to which the circulation analogs capture the anomalous winds and associated advection of 2015/16. The conclusions were found to be insensitive to the vertical level of the computed analogs and to the number of analogs (up to 10) used in computing the analog-derived temperature anomalies. While the analog circulation fields generally resemble the 2015/16 fields quite closely in both the orientation and the spacing of the isobars (height contours), there may be subtle differences that impact temperatures over Alaska. However, the local maximum of the excess warmth over the Alaskan landmass makes it doubtful that imperfect analogs are the reason why the excess warmth is such a large percentage of the observed warmth.

The 2015/16 cold season of Alaska was unprecedented in the historical record, which extends back nearly a century. The departures from climatological means were especially large in the latter portion of the cold season, January through April. Climate model simulations suggest that relative warmth of this magnitude will not become the norm until midcentury, assuming greenhouse gas emissions continue to track the scenario they are presently following. Therefore, while increasing greenhouse gas concentrations may have made a small contribution to the warmth of 2015/16, the direct radiative impact of greenhouse gases cannot explain the magnitude of the warmth.

On the basis of circulation analogs computed from sea level and 850-hPa fields, the atmospheric circulation's impact through temperature advection explains less than 50% of the anomalous warmth of 4°–5°C averaged over the seven months. The circulation-explained percentage decreased from 55% in October–December to 39% in January–April. A factor that is consistent with the seasonal and spatial patterns of the observed warmth is the anomalous surface state, including 1) ocean surface temperatures and sea ice coverage in the surrounding seas and 2) the deficient snowpack over Alaska itself. The increase of the anomalous warmth during the late winter and early spring implicates snow cover and its albedo feedback as a key player. Albedo measurements in the boreal forest and tundra biomes of Alaska confirm that the surface albedo values were lower significantly during April than in any year as far back as at least 2008, and visible images from tower cameras show an unusually dark surface even during midwinter in the boreal forest. Additional support for the role of snow cover is provided by the large-scale temperature anomaly pattern, which shows a maximum over Alaska and adjacent northwestern Canada. Of the 3°–4°C of warmth not explained by the atmospheric circulation, our best estimates are that 2°–3°C results from the surface state anomalies, while about 1°C can be explained by increased greenhouse gas concentrations. Controlled model experiments in which the lower boundary conditions are prescribed to correspond to 2015/16 and to climatology represent one approach to quantitative refinements of the impacts of snow, sea ice, and ocean temperatures. Lurking in such experiments, however, is the possibility that greenhouse warming has contributed to the anomalous surface boundary state in the Alaska region during 2015/16.

A factor not examined in this study is anomalous downwelling longwave radiation, which can be increased relative to its historical values by warmer temperatures in the lower troposphere as well as by increases in atmospheric water vapor and cloudiness. Cullather et al. (2016) show that precipitable water and cloudiness were indeed greater than normal over the Bering Sea during December–February of 2015/16, consistent with the reduced sea ice and strong southerly advection (Fig. 3). Associated anomalies of downwelling longwave radiation were deduced from AIRS data. The anomalous downwelling radiation was confined to southwestern Alaska, and its spatial pattern is consistent with the October–December excess warmth shown in Fig. 7. However, its spatial distribution does not explain the increase of excess warmth and expansion to essentially the entire state in the January–April period. To the extent that the anomalous downwelling longwave radiation can be traced to moisture originating from ocean temperature and sea ice anomalies in the Bering Sea, the seasonal and spatial patterns of the excess warmth point to an important role of SST and sea ice in the first part of the winter and an increasingly important role of snow cover during the later months. However, the contribution of the warmer air temperatures themselves to the downwelling longwave radiation remains to be determined.

It must be emphasized, however, that it is not possible to separate the greenhouse warming influence from the effects of snow, sea ice, and ocean temperatures considered in this paper. Reduced sea ice and snow cover, together with warmer ocean temperatures, are characteristics of the greenhouse warming signature of climate change in climate models. Surface boundary conditions such as these may become increasingly frequent in the future, amplifying the high-latitude warming. Attribution of a single year's anomalous warmth is confounded by the feedbacks inherent in the climate warming signal. In this respect, the most robust conclusion of the present study is that the unusual warmth of the 2015/16 cold season in Alaska cannot be explained solely by the atmospheric circulation, which has been shown here to account for slightly less than half the anomalous warmth over the 7-month period, nor does slowly varying greenhouse gas forcing explain the large magnitude of the temperature departures from their historical means. The surface state, especially of sea ice and snow cover, appears to have played a role. However, because these surface anomalies may not be independent of greenhouse warming, a fully quantitative attribution analysis requires the quantification of additional linkages, ultimately including the impact of the surface anomalies on the atmospheric circulation.

Acknowledgments. John Walsh, Brian Brettschneider, and Rick Lader were supported by the Climate Prediction Office of NOAA's Office of Oceanic and Atmospheric Research through Grants NA15OAR4310169 and NA11OAR4310141. Peter Bieniek and Rick Lader were funded by Grant/Cooperative Agreement GIOAC00588 from the U.S. Geological Survey's Alaska Climate Science Center. Eugénie Euskirchen was funded by the National Science Foundation through Grant 1107892 and by the U.S. Geological Survey Climate Effects Network. We thank Thomas Estilow of Rutgers University for providing the updated spring-season snow coverage data for Alaska. We also thank three anonymous reviewers for their helpful comments on the original manuscript.

REFERENCES

Alaska Climate Research Center, 2016: Alaska statewide climate summary. Alaska Climate Research Center, accessed 22 June 2016. [Available online at http://climate.gi.alaska.edu/statewide-archive.]

Alexander, P., and G. Gong, 2011: Modeled surface air temperature response to snow depth variability. *J. Geophys. Res.*, **116**, D14105, doi:10.1029/2010JD014908.

Bieniek, P. A., and Coauthors, 2012: Climate divisions for Alaska based on objective methods. *J. Appl. Meteor. Climatol.*, **51**, 1276–1289, doi:10.1175/JAMC-D-11-0168.1.

——, J. E. Walsh, R. L. Thoman, and U. S. Bhatt, 2014: Using climate divisions to analyze variations and trends in Alaska temperature and precipitation. *J. Climate*, **27**, 2800–2818, doi:10.1175/JCLI-D-13-00342.1.

——, U. S. Bhatt, J. E. Walsh, T. S. Rupp, J. Zhang, J. R. Krieger, and R. Lader, 2016: Dynamical downscaling of ERA-Interim temperature and precipitation for Alaska. *J. Climate Appl. Meteor.*, **55**, 635–654, doi:10.1175/JAMC-D-15-0153.1.

Bond, N. A., M. A. Cronin, H. Freeland, and N. Mantua, 2015: Causes and impacts of the 2014 warm anomaly in the NE Pacific. *Geophys. Res. Lett.*, **42**, 3414–3420, doi:10.1002/2015GL063306.

Cattiaux, J., R. Vautard, C. Cassou, P. Yiou, V. Masson-Delmotte, and F. Codron, 2010: Winter 2010 in Europe: A cold extreme in a warming climate. *Geophys. Res. Lett.*, **37**, L20704, doi:10.1029/2010GL044613.

Christidis, N., and P. A. Stott, 2012: Lengthening odds of the cold UK winter of 2010/11 attributable to human influence [in "Explaining Extreme Events of 2011 from a Climate Perspective"]. *Bull. Amer. Meteor. Soc.*, **93** (7), 1060–1061.

Cohen, J., K. Saito, and D. Entekhabi, 2001: The role of the Siberian High in Northern Hemisphere climate variability. *Geophys. Res. Lett.*, **28**, 299–302, doi:10.1029/2000GL011927.

Cullather, R. L., Y.-K. Lim, L. N. Boisvert, L. Brucker, J. N. Lee, and S. M. J. Nowicki, 2016: Analysis of the warmest Arctic winter, 2015–2016. *Geophys. Res. Lett.*, **43**, 10 808–10 816, doi:10.1002/2016GL071228.

Derksen, C., and R. Brown, 2012: Spring snow cover extent reductions in the 2008–2012 period exceeding climate model projections. *Geophys. Res. Lett.*, **39**, L19504, doi:10.1029/2012GL053387.

Estilow, T. W., A. H. Young, and D. A. Robinson, 2015: A long-term Northern Hemisphere snow cover extent data record for climate studies and monitoring. *Earth Syst. Sci. Data*, **7**, 137–142, doi:10.5194/essd-7-137-2015.

Euskirchen, E. S., A. D. McGuire, and F. S. Chapin III, 2007: Energy feedbacks of northern high-latitude ecosystems to the climate system due to reduced snow cover during the 20th century warming. *Global Change Biol.*, **13**, 2425–2438, doi:10.1111/j.1365-2486.2007.01450.x.

GISTEMP Team, 2017: GISS Surface Temperature Analysis (GISTEMP). NASA Goddard Institute for Space Studies, accessed 2 June 2016. [Available online at https://data.giss.nasa.gov/gistemp/.]

Hansen, J., R. Ruedy, M. Sato, and K. Lo, 2010: Global surface temperature change. *Rev. Geophys.*, **48**, RG4004, doi:10.1029/2010RG000345.

Hartmann, B., and G. Wendler, 2005: The significance of the 1976 Pacific climate shift in the climatology of Alaska. *J. Climate*, **18**, 4824–4839, doi:10.1175/JCLI3532.1.

Hegerl, G. C., and Coauthors, 2007: Understanding and attributing climate change. *Climate Change 2007: The Physical Science Basis*, S. Solomon et al., Eds., Cambridge University Press, 663–746. [Available online at https://www.ipcc.ch/pdf/assessment-report/ar4/wg1/ar4-wg1-chapter9.pdf.]

Hines, K. M., D. H. Bromwich, and G. J. Marshall, 2000: Artificial surface pressure trends in the NCEP–NCAR reanalysis over the Southern Ocean and Antarctica. *J. Climate*, **13**, 3940–3952, doi:10.1175/1520-0442(2000)013<3940:ASPTIT>2.0.CO;2.

Hodson, D. J. R., S. P. E. Keeley, A. West, J. Ridley, E. Hawkins, and H. T. Hewitt, 2013: Identifying uncertainties in Arctic climate change projections. *Climate Dyn.*, **40**, 2849–2865, doi:10.1007/s00382-012-1512-z.

Hoerling, M., and Coauthors, 2013: Anatomy of an extreme event. *J. Climate*, **26**, 2811–2832, doi:10.1175/JCLI-D-12-00270.1.

——, and Coauthors, 2014: Northeast Colorado extreme rains interpreted in a climate change context [in ''Explaining Extremes of 2013 from a Climate Perspective'']. *Bull. Amer. Meteor. Soc.*, **95** (9), S15–S18.

Hofmann, D. J., J. H. Butler, E. J. Dlugokencky, J. W. Elkins, K. Masarie, S. A. Montzka, and P. Tans, 2006: The role of carbon dioxide in climate forcing from 1979 to 2004: Introduction of the annual greenhouse gas index. *Tellus*, **58B**, 614–619, doi:10.1111/j.1600-0889.2006.00201.x.

IPCC, 2013: *Climate Change 2013: The Physical Science Basis*. Cambridge University Press, 1535 pp., doi:10.1017/CBO9781107415324.

Kalnay, E., and Coauthors, 1996: The NCEP/NCAR 40-Year Reanalysis Project. *Bull. Amer. Meteor. Soc.*, **77**, 437–471, doi:10.1175/1520-0477(1996)077<0437:TNYRP>2.0.CO;2.

Lader, R., U. S. Bhatt, J. E. Walsh, T. S. Rupp, and P. A. Bieniek, 2016: Two-meter temperature and precipitation from atmospheric reanalysis evaluated for Alaska. *J. Appl. Meteor. Climatol.*, **55**, 901–922, doi:10.1175/JAMC-D-15-0162.1.

Laliberté, F., S. E. L. Howell, and P. J. Kushner, 2016: Regional variability of a projected sea ice–free Arctic during the summer months. *Geophys. Res. Lett.*, **43**, 256–263, doi:10.1002/2015GL066855.

Lindsay, R., M. Wensnahan, A. Schweiger, and J. Zhang, 2014: Evaluation of seven different atmospheric reanalysis products in the Arctic. *J. Climate*, **27**, 2588–2606, doi:10.1175/JCLI-D-13-00014.1.

McAfee, S. A., 2014: Consistency and lack thereof in Pacific decadal oscillation impacts on North American winter climate. *J. Climate*, **27**, 7410–7421, doi:10.1175/JCLI-D-14-00143.1.

Meier, W. N., G. Peng, D. J. Scott, and H. M. Savoie, 2014: Verification of a new NOAA/NSIDC passive microwave sea-ice concentration climate record. *Polar Res.*, **33**, 21004, doi:10.3402/polar.v33.21004.

Melillo, J. M., T. C. Richmond, and G. W. Yohe, Eds., 2014: *Highlights of Climate Change Impacts in the United States: The Third National Climate Assessment*. U.S. Global Change Research Program, 148 pp.

Menne, M. J., and Coauthors, 2012a: Global Historical Climatology Network-Daily (GHCN-Daily), version 3. NOAA/National Climatic Data Center, doi:10.7289/V5D21VHZ.

——, I. Durre, R. S. Vose, B. E. Gleason and T. G. Houston, 2012b: An overview of the Global Historical Climatology Network-Daily database. *J. Atmos. Oceanic Technol.*, **29**, 897–910, doi:10.1175/JTECH-D-11-00103.1.

Mills, C., and J. E. Walsh, 2013: Seasonal variation and spatial patterns of the atmospheric component of the Pacific decadal oscillation. *J. Climate*, **26**, 1575–1594, doi:10.1175/JCLI-D-12-00264.1.

Mote, T. L., 2008: On the role of snow cover in depressing air temperature. *J. Appl. Meteor.*, **47**, 2008–2022, doi:10.1175/2007JAMC1823.1.

Namias, J., 1985: Some empirical evidence for the influence of snow cover on temperature and precipitation. *Mon. Wea. Rev.*, **113**, 1542–1553, doi:10.1175/1520-0493(1985)113<1542:SEEFTI>2.0.CO;2.

National Academies, 2016: *Attribution of Extreme Weather Events in the Context of Climate Change*. The National Academies Press, 165 pp., doi:10.17226/21852.

NCEI, 2016: Climate at a glance. NCEI, accessed 31 January 2017. [Available online at https://www.ncdc.noaa.gov/cag/.]

Notz, D., and J. Marotzke, 2012: Observations reveal external driver for Arctic sea-ice retreat. *Geophys. Res. Lett.*, **39**, L16502, doi:10.1029/2012GL051094.

Otto, F. E. L., N. Massey, G. J. van Oldenborgh, R. G. Jones, and M. R. Allen, 2012: Reconciling two approaches to attribution of the 2010 Russian heat wave. *Geophys. Res. Lett.*, **39**, L04702, doi:10.1029/2011GL050422.

——, S. M. Rosier, M. R. Allen, N. R. Massey, C. J. Rye, and J. I. Quintana, 2015: Attribution analysis of high precipitation events in summer in England and Wales over the last decade. *Climatic Change*, **132**, 77–91, doi:10.1007/s10584-014-1095-2.

Overland, J. E., and Overland, J. E., 2016: Recent extreme Arctic temperatures are due to a split polar vortex. *J. Climate*, **29**, 5609–5616, doi:10.1175/JCLI-D-16-0320.1.

——, ——, J. E. Walsh, and J. C. Stroeve, 2014: Future Arctic climate changes: Adaptation and mitigation time scales. *Earth's Future*, **2**, 68–74, doi:10.1002/2013EF000162.

Papineau, J. M., 2001: Wintertime temperature anomalies in Alaska correlated with ENSO and PDO. *J. Climatol.*, **21**, 1577–1592, doi:10.1002/joc.686.

Rosenblum, E., and I. Eisenman, 2016: Faster Arctic sea ice retreat in CMIP5 than in CMIP3 due to volcanoes. *J. Climate*, **29**, 9179–9188, doi:10.1175/JCLI-D-16-0391.1.

Scott, J. D., M. A. Alexander, D. R. Murray, S. Swales, and J. Eischeid, 2016: The climate change web portal: A system to access and display climate and Earth system model output from the CMIP5 archive. *Bull. Amer. Meteor. Soc.*, **97**, 523–530, doi:10.1175/BAMS-D-15-00035.1.

Seager, R., M. Hoerling, S. Schubert, H. L. Wang, B. Lyon, A. Kumar, J. Nakamura, and N. Henderson, 2015: Causes of the 2011–14 California drought. *J. Climate*, **28**, 6997–2024, doi:10.1175/JCLI-D-14-00860.1.

Shepherd, T. G., 2014: Atmospheric circulation as a source of uncertainty in climate change projections. *Nat. Geosci.*, **7**, 703–708, doi:10.1038/ngeo2253.

——, 2016: A common framework for approaches to extreme event attribution. *Curr. Climate Change Rep.*, **2**, 28–38, doi:10.1007/s40641-016-0033-y.

Shulski, M., J. Walsh, E. Stevens, and R. Thoman, 2010: Diagnosis of extended cold-season temperatures in Alaska. *Mon. Wea. Rev.*, **138**, 453–462, doi:10.1175/2009MWR3039.1.

Stewart, B. C., K. E. Kunkel, L. E. Stevens, L. Sun, and J. E. Walsh, 2013: Climate of Alaska: Regional climate trends and scenarios for the U.S. National Climate Assessment. NOAA Tech. Rep. NESDIS 142-7, 60 pp. [Available online at https://www.nesdis.noaa.gov/sites/default/files/asset/document/NOAA_NESDIS_Tech_Report_142-7-Climate_of_Alaska.pdf.]

Stott, P. A., D. A. Stone, and M. R. Allen, 2004: Human contribution to the European heat wave of 2003. *Nature*, **432**, 610–614, doi:10.1038/nature03089.

Stroeve, J. C., and D. Notz, 2015: Insights on past and future sea-ice evolution from combining observations and models. *Global Planet. Change*, **135**, 119–132, doi:10.1016/j.gloplacha.2015.10.011.

——, and ——, 2016: Corrigendum to insights on past and future sea-ice evolution from combining observations and models. *Global Planet. Change*, **144**, 270, doi:10.1016/j.gloplacha.2016.07.003.

——, V. Kattsov, A. Barrett, M. Serreze, T. Pavlova, M. Holland, and W. N. Meier, 2012: Trends in Arctic sea ice extent from CMIP5, CMIP3 and observations. *Geophys. Res. Lett.*, **39**, L15602, doi:10.1029/2012GL052676.

Trenberth, K. E., J. T. Fasullo, and T. G. Shepherd, 2015: Attribution of climate extreme events. *Nat. Climate Change*, **5**, 725–730, doi:10.1038/nclimate2657.

Van Oldenborgh, G. J., R. Haarsma, H. De Vries, and M. R. Allen, 2015: Cold extremes in North America vs. mild weather in Europe: The winter of 2013–14 in the context of a warming world. *Bull. Amer. Meteor. Soc.*, **96**, 707–714, doi:10.1175/BAMS-D-14-00036.1.

Walsh, J. E., and B. Ross, 1988: Sensitivity of 30-day dynamical forecasts to continental snow cover. *J. Climate*, **1**, 739–754, doi:10.1175/1520-0442(1988)001<0739:SODDFT>2.0.CO;2.

Wolter, K., M. Hoerling, J. K. Eisheid, G. J. van Oldenborgh, X.-W. Quan, J. E. Walsh, T. N. Chase, and R. M. Dole, 2015: How unusual was the cold winter of 2013/14 in the upper Midwest? [in ''Explaining Extreme Events of 2014 from a Climate Perspective'']. *Bull. Amer. Meteor. Soc.*, **96** (12), S10–S14.

Yiou, P., R. Vautard, P. Naveau, and C. Cassou, 2007: Inconsistency between atmospheric dynamics and temperatures during the exceptional 2006/2007 fall/winter and recent warming in Europe. *Geophys. Res. Lett.*, **34**, L21808, doi:10.1029/2007GL031981.